Coseismic Fault Rupture Detection and Slip Measurement by ASAR Precise Correlation Using Coherence Maximization: Application to a North–South Blind Fault in the Vicinity of Bam (Iran)

F. Sarti, Pierre Briole, M. Pirri

Submitted to *IEEE Geoscience and Remote Sensing Letters* (GRSL), GRSL-00082-2004

Co-seismic fault rupture detection and slip measurement by ASAR precise correlation using coherency maximization. Application to a North-South blind fault in the vicinity of Bam (Iran).

Francesco SARTI[1], Pierre BRIOLE[2], Mauro PIRRI[3]

[1]ESA/ESRIN, V.G.Galilei, 00044 Frascati, Italy. Phone +390694180409, mail : francesco.sarti@esa.int
[2]IPGP, 4 Place Jussieu, 75005 Paris, France. Phone +33144 27 48 93, mail : briole@ipgp.jussieu.fr
[3]TELESPAZIO, C.S.M., c. Terlecchia, 75100 Matera, Italy. Phone +39835377402, mail : mauro_pirri@telespazio.it

ABSTRACT

Using the phase differences between satellite radar images recorded before and after an earthquake, interferometry allows mapping the projection along the line of sight of the ground displacement. Acquisitions along multiple lines of sight theoretically allow deriving the complete deformation vector, however, due to the orbit inclination of current radar satellites, accuracy is poor in the North-South direction. Moreover, large deformation gradients (*e.g.* fault ruptures) prevent phase identification and unwrapping and cannot be measured directly by interferometry. Sub-pixel correlation techniques using the amplitude of the radar images allow measuring such gradients, both in slant-range and in azimuth. In this paper, we present a correlation technique based on the maximization of coherency for a radar pair in interferometric conditions, using the complex nature of the data. In the case of highly coherent areas, this technique allows estimating the relative deformation between images. Applied to ASAR (ENVISAT) images acquired before and after the 26 December 2003 Bam earthquake (Iran), we show that the near-field information retrieved by this technique is useful to constrain geophysical models. In particular, we confirm that the major gradients of ground displacement do not occur across the known fault scarp but ~3km west of it and we also estimate directly the amplitude of right lateral slip, while retrieving this value from interferometry requires passing through the use of a model for the earthquake fault and slip.

INTRODUCTION

Satellite radar interferometry can provide a spatially continuous measurement of deformation fields over large areas, with accuracy of the order of a few millimetres in the case of C-band SAR (*Massonnet and Feigl, 1998*). This has allowed capturing displacement fields of earthquakes like Landers (*Massonnet et al., 1993*), Northridge (*Massonnet et al., 1996*) and more recently Izmit (*Feigl et al., 2002*). Interferometry has two major limitations: (1) the biases due to troposphere and ionosphere heterogeneities between acquisitions; (2) the loss of coherency due to geometric decorrelation (large baselines, slopes oriented to the satellite pass) or temporal decorrelation (water, snow, vegetation and agriculture, areas where human activity, erosion or shaking effects have modified the position of elementary backscatterers within a cell).

The separation of atmospheric delays from ground displacements is discussed in several papers (*e.g. Rigo and Massonnet, 1999; Feigl et al., 2002*). When no external information is used, it requires several interferograms of the same area. Separation can prove very successful especially in flat and urban areas (e.g. *Fruneau and Sarti, 2000*). Coherency loss due to changes of the ground, instead, is not recoverable, except when it derives from de-registration (*Deraw 1999; Michel et al., 1999b*). A way to overcome coherency and atmosphere limitations is the powerful technique of Permanent Scatterers (PS), but since it requires large a data archive and sufficient scatterers density, its use remains confined mostly to urban areas.

Even when coherency is preserved, phase-based techniques are not adapted for measuring large deformation gradients (*i.e.* 0.5 fringes/pixel or more): in this case, phase recognition and unwrapping become impossible unless some lower frequency components of the deformation are known *a priori* and can be removed in order to reduce the gradients.

GEOMETRICAL LIMITS OF 3-D DISPLACEMENT FIELDS RETRIEVAL FROM INTERFEROMETRY

Phase-based interferometric techniques measure variations along the radar line of sight (slant range) and are not sensitive to variations perpendicular to this direction (azimuth). In the case of near-polar satellites orbits, this induces a low capability to detect North-South ground motions (except at very high latitudes). Following the notation used by *Wright et al.,* (2004), let $\boldsymbol{d} = (d_x\ d_y\ d_z)^T$ be the vector of East, North and Vertical displacements of a point at the Earth surface, and $\boldsymbol{v} = (v_x\ v_y\ v_z)^T$ the unit line of sight (LOS) vector (also called *sensitivity vector*) expressed in the same local

reference system as **d** and pointing from the ground to the satellite (Fig.1). The range change is the scalar product of **d** and $\boldsymbol{v}$:

$$r = -\boldsymbol{v}^T \boldsymbol{d} \qquad (1)$$

A typical value of $\boldsymbol{v}$ for ENVISAT IS2 mode on a descending orbit and at medium latitudes is (0.33, -0.07, 0.94). In this mode (which has the same 23° incidence angle as ERS), interferograms have a high sensitivity to the vertical component of deformation, a medium East-West sensitivity, and a very low North-South sensitivity. At higher incidence modes (*e.g.* ENVISAT IS7) the East-West sensitivity increases at the expense of the Vertical one but the North-South one remains low.

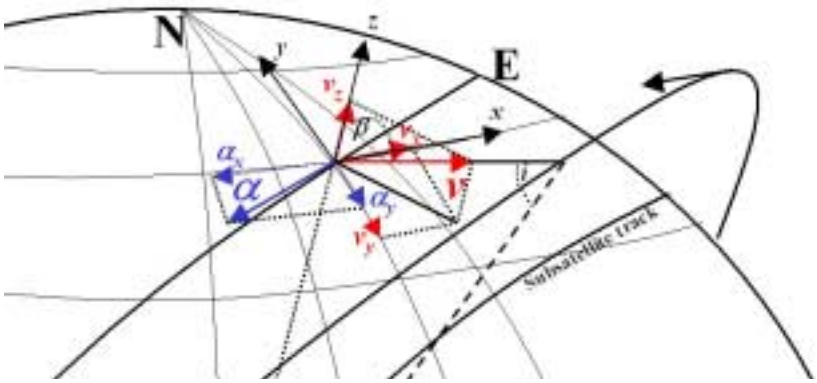

Fig1. Geometry of acquisition, descending SAR orbit (for the purpose of a clearer representation, the orbit inclination has been exaggerated: -140° rather than –98°)

Theoretically, using interferograms obtained with images acquired from N≥3 independent look directions (*e.g.* from ENVISAT orbits with different acquisition modes), (1) becomes a resolvable system of N equations. The three components of the displacement $\boldsymbol{d}$ can be obtained by inversion. *Wright et al.,* (2004) show that, assuming a constant range error σ on each look direction, the covariance matrix $\boldsymbol{\Sigma}$ associated to the weighted least squares solution is:

$$\boldsymbol{\Sigma} = \sigma\ (\boldsymbol{V}^T \boldsymbol{V})^{-1} \qquad (2)$$

where $\boldsymbol{V}$ is the N x 3 matrix $(\boldsymbol{v}_1^T, \boldsymbol{v}_2^T, .. \boldsymbol{v}_N^T)^T$ and σ is a scalar. In the case of the IS2 and IS7 ascending and descending ENVISAT modes (N=4 look directions), the same authors show that the standard error of the measurement along the North-South axis computed from $\boldsymbol{\Sigma}$ is roughly10 times larger than the other two components. This is due to the small angular separations between IS2 and IS7 incidences (~20°) and between ascending and descending tracks (~18° at the equator). Therefore, although N≥3 different ENVISAT look directions theoretically allows retrieving 3-D motions, in practice additional information (e.g. GPS, in-situ data, optical and/or radar correlation results) is fundamental to really infer 3-D displacement fields. *Feigl et al.* (2002) show such an example of inversion from multiple data sources.

FINE RADAR CORRELATION (FRC) IN INTERFEROMETRIC CONDITIONS

While interferometric phase between two radar acquisitions allows measuring a variation of distance along the line of sight, the whole complex signal (intensity and phase) can be used to estimate the component of the relative deformation perpendicularly to the line of sight. Applied to radar pairs in interferometric conditions, fine radar correlation (FRC) provides information about the shifts in range (image columns) and azimuth (image lines) between the images. In the processing chains used for interferometry, precise co-registration is usually obtained by sub-pixel correlation of the two images using cross-correlation of multi-looked radar intensities, i.e. image features. Although the required co-registration accuracy for interferometry is ~0.3 pixels, much better accuracies can be achieved locally by FRC when the coherency is high, taking advantage of speckle conservation and phase pattern preservation between acquisitions in the case of a small baseline (same incidence). According to *Bamler* (1999), the standard deviation σ of the measured shift $\delta_{r,a}$ (in *range* or in *azimuth*) resulting from optimal estimation (maximum likelihood) applied to a complex radar pair in interferometric conditions is :

$$\sigma(\delta_{r,a}) = \frac{\sqrt{3}}{\sqrt{2N}} \frac{\sqrt{1-\gamma^2}}{\pi\gamma} \tau_{r,a}^{3/2} \qquad (3)$$

This standard deviation represents the ultimate accuracy achievable by precise correlation using *complex* data and it is a lower bound for the error of any estimator. In (3), σ is expressed as a fractional number of pixels, N is the number of samples in an estimation window, γ *is* the local coherency value and τ is the oversampling factor of radar data (sensor resolution expressed in number of pixels). This latter value is a system parameter, depending on the instrument and the synthesis applied (in particular, on the processed bandwidth, for τ_a). For ASAR IMS IS2, τ_a = 1.23 pixels and τ_r = 1.18 pixels. Coherency can be partially improved by using a common Doppler and bandwidth at synthesis level but the improvement is marginal for a stable Doppler system like ENVISAT. With N=25000 samples, (3) yields values of σ varying between 0.0032 and 0.0016 pixels for coherency values between 0.5 and 0.8. N must be limited in order to account for spatial variations of the displacement, which, ideally, should remain constant within one estimation window. Therefore, in regions of high local deformation gradients (e.g. close to a seismic fault) N has to be reduced (typically, N=2500) and σ is larger. In the case of the Bam earthquake discussed below, having applied FRC to ASAR data, we estimate σ to be of the order of 0.02 pixels (in areas of low deformation gradient), *i.e.* an accuracy in deformation detection 2-3 orders of magnitude larger than with interferometry. FRC is thus far less precise than interferometry but robust and well suited for the detection of large (metric or so) deformation, like near-field co-seismic displacements or volcano deformation.

In the literature, several examples of FRC can be found. Some authors estimated the optimum shift by maximization of a cross-correlation function using up-sampled intensity data. In this case, complex radar data are up-sampled by zero-padding (prior to intensity correlation), as well as the cross-correlation function itself (*Gray et al.*, 2001). These authors call this technique *speckle tracking* because fine correlation is obtained thanks to the conservation of the high-frequency speckle pattern between the two images rather than to landscape morphology. A normalized function in the Fourier transform domain, called Symmetrical Phase-Only Filter, for the precise correlation of radar intensities, was used by *Michel et al.* (1999a) to map the fault rupture for the Landers earthquake observed by ERS. A more recent application of this technique, also using radar intensity, was shown by *Fialko et al.* (2001).

Correlating directly *complex* radar data has the advantage that over-sampling prior to correlation is not necessary, since the total information of intensity and phase is conserved. This technique was used by *Deraw* (1999) for the estimation of the displacement field of a glacier from an ERS tandem pair, using the principle of coherency maximization.

Here, we use a 2-step approach with a first estimate of the shift performed by radar intensity correlation and a further refinement based on complex data correlation (algorithm implemented in the software BEST, distributed by ESA). In both steps, maximization is performed in the frequency domain.

1. Cross-correlation between the two single-look radar intensities I_1, I_2 (of the master and slave acquisitions *M*, *S* respectively) is used in order to achieve an initial coregistration. The optimum shifts (δc, δr) in row and columns are found by searching the peak of the cross-correlation in the spectral domain on a grid of ground control points (GCP):

$$Max_{\delta c,\, \delta r} \; FT^{-1}\{FT(I_1(c,r))\,[FT(I_2(c-\delta c,\, r-\delta r))]^*\} \qquad (4)$$

The two transforms $FT(I_1)$, $FT(I_2)$ are interpolated in the spectral domain by zero-padding in order to achieve sub-pixel accuracy. An advantage of the frequency domain is that a spatial shift corresponds to a phase rotation whereas the spectrum is unchanged:

$$FT(A(n-\Delta n)) = FT(A(n))\, e^{-j\, k\, \Delta n\, 2\pi/N} \qquad (5)$$

N is still the number of samples in the estimation window and k is the variable in the discrete transform domain. Aberrant estimation values or points corresponding to a correlation rate below a threshold are eliminated. The first step can be reiterated, starting with a new shift estimation after having corrected the GCP position on the slave image using the previous estimates. The percentage of false cross-correlation points decreases from 20% (one iteration) to 5% (two iterations) for a typical case.

2. After a first image coregistration based on (4), a fine coregistration process can start, based on the *complex* data *M*, *S*. The principle is the maximization of coherency estimation by application of an optimum shift to the co-registration. The shift corresponding to the peak of the following function has to be determined:

$$\max_{\delta c,\delta r} \frac{\left|E\{M\ S^*\}\right|}{\sqrt{E\{I_1^{\ 2}\}E\{I_2^{\ 2}\}}} = \frac{\left|\Sigma\Sigma\{M(c,r)[S(c-\delta c, r-\delta r)]^*\}\right|}{\sqrt{\Sigma\Sigma[I_1^{\ 2}(c,r)]\Sigma\Sigma[I_2^{\ 2}(c-\delta c, r-\delta r)]}} \quad (6)$$

In this expression, E{} is the *expectation value* and the summations Σ are performed for all columns, rows in each finite estimation window centred on the GCP. In order to obtain uncorrelated estimation values, the distance between grid points should not be smaller that the size of an estimation window. As a result of this maximization, two images (range shifts and azimuth shifts) are obtained, with the same dimension as the grid used for the solution of (6).

RETRIEVAL OF 3-D DISPLACEMENT FIELDS FROM FINE RADAR CORRELATION

As shown in the previous section, fine radar correlation (FRC) yields two measurements, the column shift δc (slant range displacement), which has the same sensitivity vector $\boldsymbol{v}$ as the interferometric measurement, and the row shift δr (azimuth displacement), which measures mainly the North-South component, poorly observable by interferometry. In order to translate these shifts into ground displacements, several corrections are necessary: (i) relative deformation between master and slave images due to little stereoscopic effects on areas of relief; (ii) orbit rotation between master and slave passes; (iii) shift biases in azimuth and range linked to orbital errors and inexact start-time and *near range* annotations in the products. The first two corrections (i) and (ii) use a model based on topography and precise orbits. For the third one (iii), the mean azimuth and range shift are computed from the result of (6) and then subtracted.
A geometric projection from range and azimuth axes to a local reference frame has then to be performed. The unit vector in the azimuth direction on the ground can be expressed in a local reference system by its East, North and Vertical components $\boldsymbol{\alpha}=(\alpha_x\ \alpha_y\ 0)^T$(Fig.1). Let us call $r_c = \delta_r\rho_r$ and $a_c = \delta_a\rho_a$ the measurements of the shift in range and in azimuth ($\rho_{r,a}$ = pixel size in range or in azimuth), after topographic and roto-translational effects correction. The following equations hold:

$$r_c = -\boldsymbol{v}^T\boldsymbol{d} \quad (7)$$
$$a_c = \boldsymbol{\alpha}^T\boldsymbol{d} \quad (8)$$

Equations (1), (7), (8) do not allow for a 3-D inversion of the displacement vector because both r and r_c measure the projection of the displacement along the same LOS direction (range change), obtained with different methods and accuracies. As already mentioned, the accuracy σ achieved in the estimation of the range shift (7) is at least two orders of magnitude larger than with interferometry (1). Moreover, unless a deformation model is available, a direct combination of interferometric measurements and radar correlation results is not possible in general because these techniques are applicable on complementary regions: correlation is applied where the deformation gradient is usually too high to allow interferometric observation.
In case both a descending and an ascending pairs are available, precise correlation can be applied to both. A system of 4 independent equations is obtained from (7) and (8), allowing the derivation of $\boldsymbol{d}$ as the solution of a least-squares problem. Assuming a similar accuracy σ in the shift determination on different axes[1], the covariance matrix has the same form as (2), where $\boldsymbol{V}$ is now the 4 x 3 matrix $(\boldsymbol{v}_1^T, \boldsymbol{v}_2^T, -\boldsymbol{\alpha}_1^T, -\boldsymbol{\alpha}_2^T)^T$. Differently from the case of a combination of several interferograms with different look directions, the orthogonality between azimuth and range directions for each pair and the good angular separation (>40 degrees) between ascending and descending LOS directions ensures now favourable conditions for an inversion of the deformation vector.

An example of 3-D displacement field derivation from integration of SAR amplitude correlation and interferometry applied to ERS ascending and descending passes is shown by *Fialko et al.* (2001), for the Hector Mine earthquake.

APPLICATION TO THE BAM EARTHQUAKE DISPLACEMENT FIELD

On December 26th, 2003, an M_ω6.5 earthquake destroyed the historical city of Bam (Southeast Iran). Several co-seismic interferograms were formed from ENVISAT ASAR acquisitions. Here, we consider the co-seismic descending pair ASAR IS2 9192 (Dec. 3rd, 2003) – 10194 (Feb. 11th, 2004) with a 70-day time interval and a baseline of a few meters. Apart from the cities of Bam and Baravat (presence of vegetation and a high level of urban damage), the overall

[1] in practice, this is normally not the case because $\rho_r > \rho_a$ and $\tau_a \cong \tau_r$

coherence is high thanks to the small orbit baseline and the dry arid region, Fig.2(b) and 3(a). These conditions guarantee the speckle conservation, which is a prerequisite for the application of precise correlation techniques. Shift estimation was performed for the areas outside the coherency mask, exhibiting an average coherency of 0.8.

Southeast Iran contains several fault systems like Nayband-Gowk-Sabzevaran and Dash-e Lut with quasi-North-South orientation (*Talebian, et al, 2004*). A previously known fault, running North-South on the western edge of Bavarat is clearly visible on the SPOT-5 image, Fig.3(b). A coseismic fault slip parallel to this fault would be poorly observable on the interferogram, because of its geometry. Azimuth shift estimation was therefore attempted, using the algorithm (4), (5), (6). Correction of topography and roto-translation effects (i), (ii), (iii) was then performed. Rotation effects were linked to orbit crossing and orbit control maneuvers performed by ESOC on February 5th, targeted to orbit baseline minimization over Bam. The result of azimuth shift estimation after these corrections is shown in Fig.2(c). This image shows a previously unknown rupture, southern of the city of Bam, separating upward displacements (on the West) from downward ones (on the East). The segment detected, PQ, can be recognized on the coherency image, Fig.2(b), because of local decorrelation. A precise localisation is not possible on these images because of their low resolution (images computed on the points of a grid). For this reason, we computed a full resolution coherency image, shown in Fig.3(a), using the precise coregistration which is possible at the end of the precise correlation process (6). One should stress the fact, however, that though useful for localisation purposes, coherency alone would not be sufficient for the identification of the fault rupture. Many other incoherent features appear, apart from the fault itself. It is only by a combined inspection of azimuth shift, range shift, and coherency that this identification is possible.

Neither radar intensity nor the optical images could support fault detection in this particular case because of the complete absence of geomorphological features associated. *Talebian, et al.,* (2004), show evidence of a rupture on the ground, with an offset of the order of 20cm in a right lateral sense, with the same location as that shown by our analysis. This rupture is traced on the SPOT-5 image, Fig.3(b). It runs parallel to the old fault, 4km on the West. On the interferogram, Fig.2(a), this location corresponds to dense fringes, implying a high deformation gradient in range. The result of range shift estimation is shown in Fig.2(d). Also in this case, roto-translational and topographic effects were subtracted. Though with a lower SNR, this result is consistent with the hypothesis of a rupture: a discontinuity exists between eastward and westward displacements. A composition of the azimuth and the range components of the displacement confirms a right lateral slip, parallel to the detected rupture. Because of the slant-range geometry and the sensitivity of range shift to both vertical and East-West deformation, we cannot exclude the existence of a vertical component as well. In order to attempt a *quantitative* estimation, azimuth shift profiles have been traced along 9 line segments across the fault, plotted in Fig. 2(b).
These segments range from AD down to BC and cover the whole rupture PQ. Each segment is 6.8 km long in slant range (17.5km when ground-projected). A series of profiles are shown in Fig.4, vertically interspaced by 1140m. The azimuth profiles clearly show a discontinuity and a sign inversion at the fault crossing. Their mean slope gives the deformation gradient. A maximum offset (total excursion between minimum and maximum) close to 1m can be measured in the azimuth shift profiles close to Bam (AD segment, point P), whereas this offset decreases to less than 0.6m in the South (BC segment, point Q). The maximum and the minimum on a profile are separated by roughly 2km. Range profiles (not displayed) exhibit an increasing offset when moving southwards from the AD profile down to the BC one; however, the measurement on these profiles is close to the noise level. The SNR in range is much lower than in azimuth. This is consistent with (3), which predicts $\sigma_r \approx 2\sigma_a$ (in meters).

With a mean coherency of 0.811 in the fault area (ABCD), (3) yields a best accuracy of 0.004 pixels. In order to estimate the accuracy of the technique applied to the ASAR pair, we computed the standard deviation of the shift measurement in areas far from the fault rupture and with the same mean coherency. In order to avoid topographic effect, flat areas were selected: a homogeneous displacement field can be expected and the standard deviation of the shift can be used to measure the noise of the estimate. Values found are close to 0.02 pixels in azimuth (10cm) and 0.015 pixels in slant range (13cm), 3-4 times larger than the theoretical value given by (3). This is a satisfactory result. Real accuracy for the shift estimate when approaching the fault rupture will be higher than this value because of non-linear displacements, discontinuities (on the rupture itself) and local coherency decrease.
Standard deviation could be reduced by averaging these profiles on segments normal to the fault, provided the displacement as a function of the distance from the fault stays the same between close enough segments.

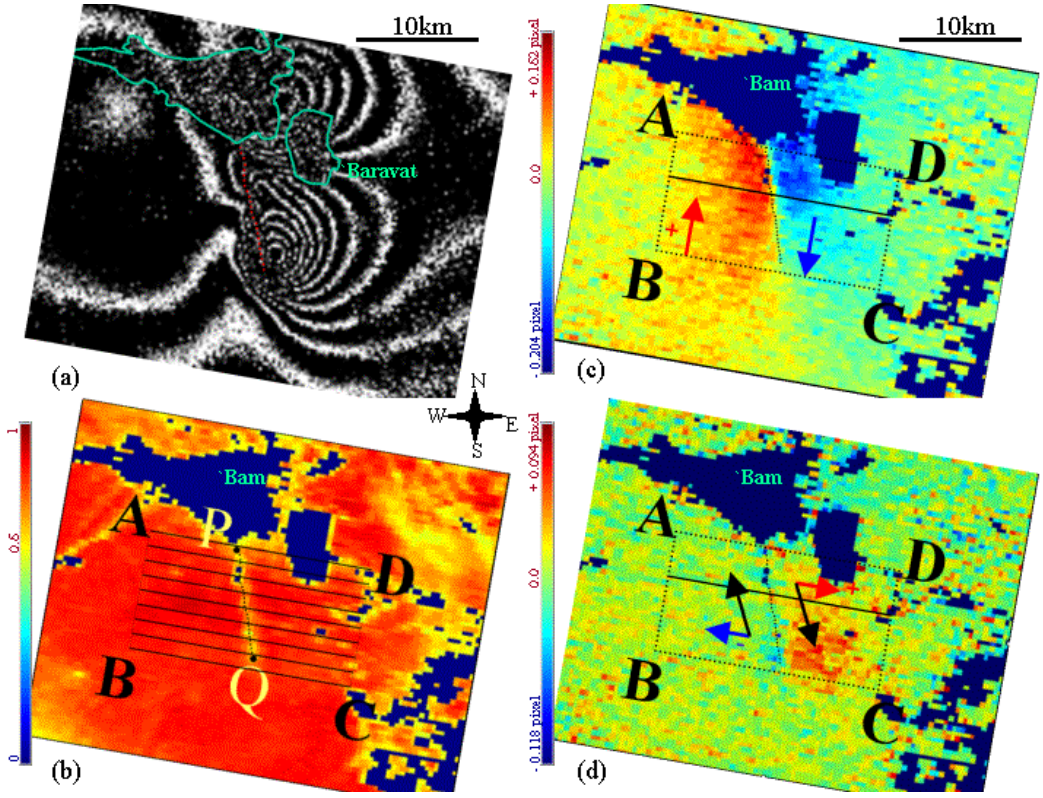

Figure 2. Co-seismic ASAR pair IS2 9192 (Dec. 3rd, 2003) – 10194 (Feb. 11th, 2004). Results from interferometry (a), coherency (b), azimuth shift estimation (c), range shift estimation (d) based on radar intensity correlation followed by *coherency maximization*. Reduced spatial resolution of these images derives from the fact they were computed on the points of a grid with a pixel spacing such that shift estimates are independent. Images (b), (c), (d) are masked for coherency values lower than 0.6. Joint use of azimuth correlation and coherency allows fault mapping. This fault segment is then retraced on a SPOT-5 image, Fig.2(b), allowing a better geodetic localization. Though with a lower SNR, range shift estimation confirms a fault rupture at the same location. Combination of the two orthogonal measurements yields a right-lateral slip, parallel to the fault rupture (black arrows). This rupture corresponds to a *blind fault,* with no associated morphological features. Ground evidence for this fault was collected by *Talebian, et al. (2004*).

GEOPHYSICAL INTERPRETATION

In a previous study based in the analysis of InSAR data, *Talebian et al.,* (2004) have shown that the amplitude of the interferogram and the spatial extension of the fringes imply that the slip on the fault is between 1.5 and 2m, at a depth between 10-12 and 1-2 km. These authors suggest that the slip might decrease between 1-2 km depth and the surface, reaching ~20cm at the surface (i.e. a value compatible with field observation of ground rupture), where anomalous coherence in InSAR data analysis is cleary observable (Figure 3). The shift of the newly active fault, ~4km westward with respect to the "old" fault marking the topography, already observed by InSAR (*Talebian et al.,* 2004) is also observed with our data. The interpretation of these authors for the offset is the possible existence of a shallow sub-horizontal *decollement* layer connecting the "new" fault at a depth of ~2km to the surface, like that already proposed for the Fandoka earthquake (*Berberian et al., 2001*).

In order to test our results against a model, we plotted azimuth and range offsets along eight profiles in the area of maximum deformation (Figure 4). We then used a model fitting well the InSAR data (close to the model of *Talebian et al.,* (2004) to predict the theoretical azimuth and range offsets. The parameters of the model used are summarized in Table 1.

Center of the upper fault edge (UTM40_E)	Center of the upper fault edge (UTM40_N)	Depth of the upper fault edge	Fault azimuth	Fault half length	Fault width	Dip angle	Strike slip
631.45	3213.35	1	N5°E	6.	13.	90°	2.0 m

Table 1: Parameters of the modeled fault

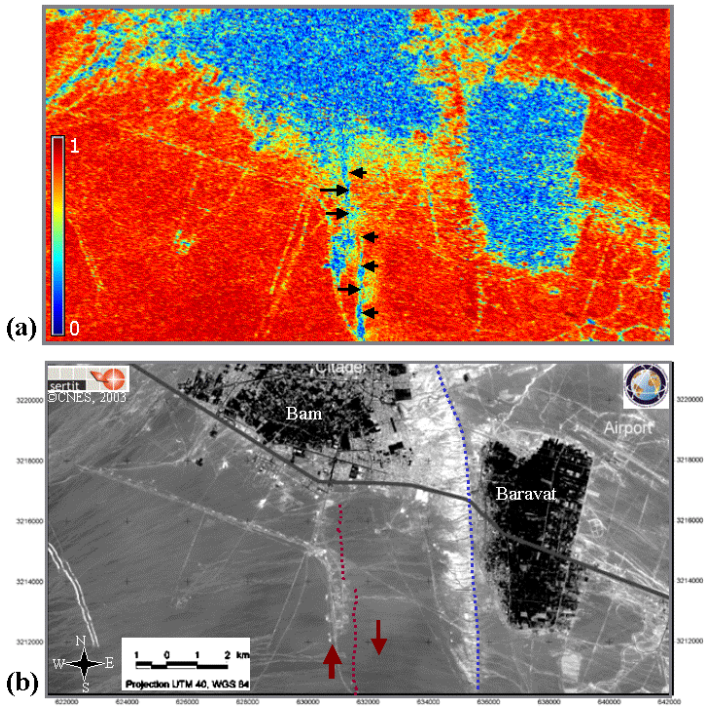

Figure 3: Bam and Bavarat region. (a) Coherency image obtained after fine coregistration (full resolution). The discontinuity in the azimuth shift estimation can be identified in this image and traced on the SPOT-5 image. (b) Space Map realised from a SPOT-5 image acquired Oct 21st 2003, within an activation of the International Charter "Space and Major Disasters". Black areas indicate the presence of vegetation. The fault known in the topography is plotted with a blue dashed line close to Baravat. Though many features can be recognised from a comparison of (a) and (b), there is no feature on the SPOT-5 image corresponding to the new fault rupture (red dashed line) detected by means of radar correlation. Its right-lateral slip, measured from azimuth & range shift estimation, is marked with red arrows. The new fault runs parallel to the old one and is located 4km more on the West.

Figure 5 presents the theoretical azimuth and range offsets. The main result in terms of fault model is the fact that our data can be fitted correctly only when the rupture arrives very close to the ground surface. In the model of Table 1, the predicted offsets are about half of the observed ones; this discrepancy reduces to 30% when the upper part of the fault is assumed to be at 0.5km depth only, implying that the upper edge should be even shallower than 0.5km. We did not perform tests with the upper part of the fault shallower than 0.5km for two reasons: (i) at a shallower depth, the fit between our data and the model improves but at the same time the fit between predicted and observed interferograms degrades; (ii) at such shallow depth, modeling the dislocation of the Earth crust with the simple theory of dislocation in a elastic half-space becomes insufficient. In all cases, our data imply that the slip on the fault must remain large – more than 1m - on the fault plane down to a few hundred of meters below the surface. This result might have some impact on the assumption of existence of a sub-horizontal *decollement* connecting "new" and "old" fault. Indeed, in this theory, there is no need for the slip to remain high at low depth since the deformation is transferred laterally towards east along the sub-horizontal plane. Since our data show that the slip on the fault remains high up to very shallow depth, the model implying a sub-horizontal *decollement* is therefore weakened, although we have no alternative explanation for the fact that "new" and "old" fault are not located at the same place.

CONCLUSIONS AND PERSPECTIVES

The enhanced precision of new radar correlation techniques opens the possibility to combine radar interferometry and bi-dimensional shift measurement for the modelling of large ground deformation, like those associated to seismic or volcanic phenomena. Application to ASAR in interferometric conditions allowed mapping a new blind fault close to Bam. Here we demonstrate that not only detection but also fault slip measurement is possible with this technique: correlation accuracies close to 0.02 pixels are achieved in areas of linear displacements, thus approaching the theoretical limit. This direct measurement of the slip along the fault complements the high-precision results of radar interferometry

far from the fault region and gives better insight of the fault model. The main result obtained is that the fault rupture is closer to the ground surface than previously estimated using InSAR only.
With accuracies between 1/10 and 1/100 of a pixel and the advent of higher-resolution SAR systems like RADARSAT-2 (3m) these techniques become even more promising.

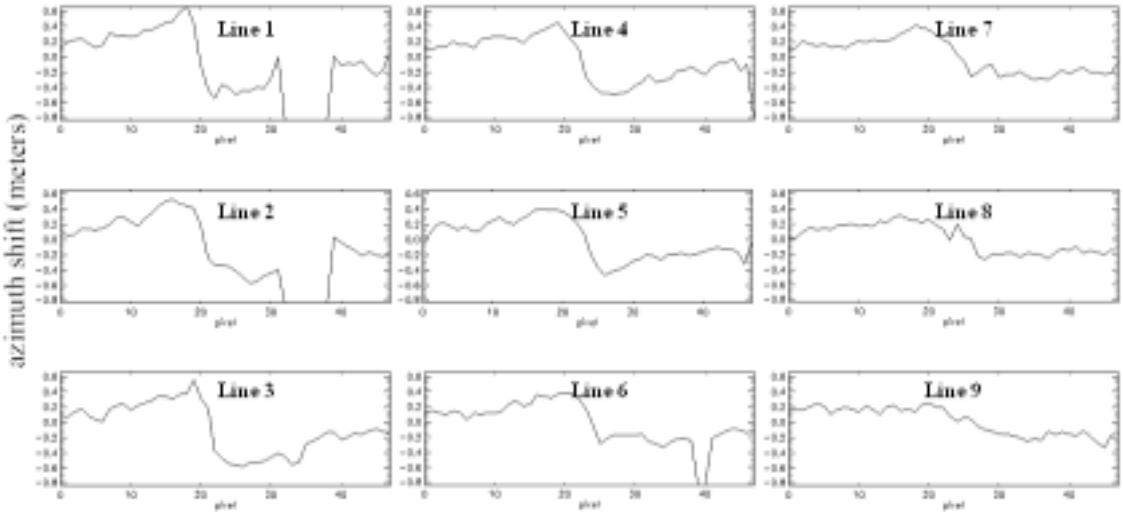

Figure 4. Profiles of displacement in azimuth. Computed on horizontal segments across the fault in a rectangle ABCD (compare to Fig.1(b)): line 1 is the segment AD, line 9 is the segment BC. The excursion for each profile gives an estimate of the slip. The displacement in range is close to the noise level (not displayed). The standard deviation far from the fault area is lower than 0.02 pixels, thus approaching the theoretical limit allowed by radar correlation.

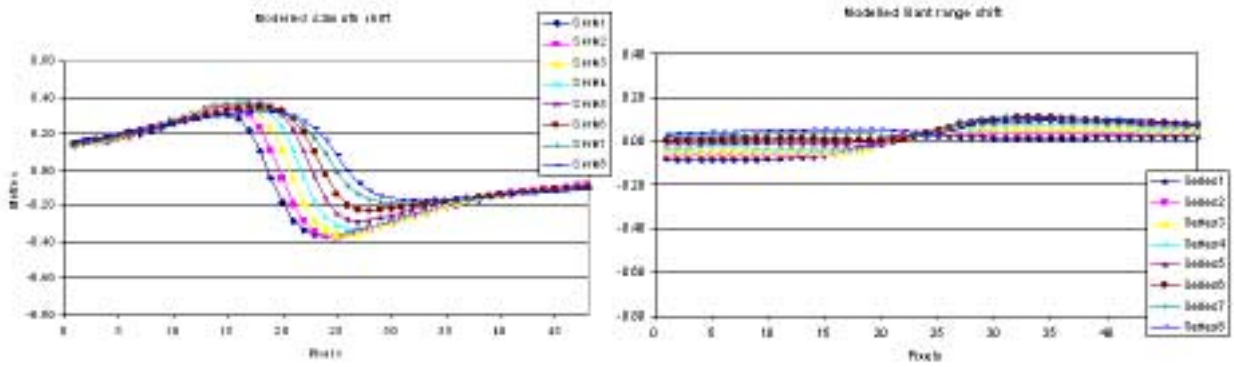

Figure 5. Profiles of displacement in azimuth (top) and range (bottom) computed on the same segments as for Figure 4. The parameters of the fault model used for this simulation are given in Table 1. The wavelengths of the observed and modelled deformation are close, but the amplitude of the observed offsets is larger than the modelled one. This implies that the upper edge of the fault is very shallow, between 0.5 and 0.2km depth. In order to fit the observed azimuth offsets, the slip on the fault must remain large on the uppermost part of the fault, typically between 1.5 and 2m slip.

ACKNOWLEDGEMENTS

We thank the European Space Agency for providing the ASAR dataset over the region of Bam, as well for the software tools (BEST) allowing the computation of precise correlation results for this work.

REFERENCES

Bamler, R., (1999), Interferometric Stereo Radargrammetry: Absolute Height Determination from ERS-ENVISAT Interferograms. Proc. of IGARSS'99 (Hamburg), Vol.3, pp.1517-1521

Berberian, M., C. Baker, E. Fielding, J. Jackson, B. Parsons, K. Priestley, M. Qorashi, M. Talebian, R. Walker, and T. Wright (2001), The 14 March

1998 Fandoqa earthquake (Mw 6.6) in Kerman province, S.E. Iran: Re-rupture of the 1981 Sirch earthquake fault, triggering of slip on adjacent thrusts, and the active tectonics of the Gowk fault zone, Geophys. J. Int., 146, 371–398.

Deraw, D., (1999), Dinsar and coherence tracking applied to glaciology: the example of the Shirase Glacier. Fringe meeting 1999, Liège

Feigl K., Sarti, F., et al. (2002). Estimating slip distribution for the Izmit mainshock from coseismic GPS, SPOT and ERS-1 measurement. Bulletin of the Seismological Society of America, special issue on Izmit and Duzce Turkey Earthquakes, 92, 1, pp.138-160, February 2002

Fialko, Y., et al., (2001). The complete (3-D) surface displacement field in the epicentral area of the 1999 Mw 7.1 Hector Mine earthquake, California, from space geodetic observations. Geo. Res. Letters, 28(16), 3063-3066

Fruneau. B., Sarti, F. (2000). Detection of Ground Subsidence on the City of Paris Using Radar Interferometry: isolation of deformation from atmospheric artefacts using correlation. Geoph. Res. Letters, vol.27, n.24, p.3981

Gray, A.L., Mattar, K.E. and Sofko, G., (2000). Influence of Ionospheric Electron Density Fluctuations on Satellite Radar Interferometry. Geoph. Res. Letters, Vol. 27, No. 10, pp. 1451-1454

Gray A. L., Short N. , Mattar K. E., Jezek K. C., (2001). Velocities and Flux of the Filchner Ice Shelf and its Tributaries Determined from Speckle Tracking Interferometry. Canadian J. of Remote Sensing , vol. 27, no. 3

Massonnet, D. & Feigl, K. (1998). Radar interferometry and its application to changes in the earth surface. Rev. of Geoph., Vol. 36, 4 pp. 441-500.

Massonnet, D., K. Feigl, H. Vadon, M. Rossi (1996). Coseismic deformation field of the M = 6.7 Northridge, California earthquake of January 17, 1994 recorded by two radar satellites using interferometry. Geoph. Res. Letters, 23 (9), 969-972.

Massonnet D., et al., (1993). The displacement field of the Landers earthquake mapped by radar interferometry. Nature, 364, p. 138-142.

Michel, R., Avouac, J.P., Taboury (1999a). Measuring ground displacements from SAR amplitude images: application to the Landers earthquake. Geoph. Res. Letters, vol. 26, n.7, 875-878

Michel, R., Avouac, J.P., Taboury (1999b). Measuring near-field coseismic displacements from SAR images: application to the Landers earthquake. Geoph. Res. Letters, vol. 26, n.19, pages 3017-3020

Rigo, A., and D. Massonnet (1999). Investigating the 1996 Pyrenean earthquake (France) with SAR Interferograms heavily distorted by atmosphere. Geoph. Res. Letters, 26, 3217-3220

Talebian, M., et al., (2004). The 2003 Bam (Iran) earthquake – rupture of a blind strike-slip fault. Geoph. Res. Letters, to appear, DOI:10.1029/

Vadon, H., Massonnet, D., (2000). Earthquake displacement fields mapped by very precise correlation: complementarity with radar interferometry. IEEE International Geoscience Remote Sensing Symp., Honolulu, Hawaii, 24–28 July 2000, IEEE Periodicals, Piscataway, New Jersey, 2700–2702.

Wright T.J., et al.(2004). Toward mapping surface deformation in three dimensions using InSAR. Geo. Res. Letters, Vol.31.